J. Fluid Mech. (2011), *vol.* 666, *pp.* 414–427.
doi:10.1017/S002211201000491X

Leakage from gravity currents in a porous medium. Part 2. A line sink

DOMINIC VELLA†, JEROME A. NEUFELD, HERBERT E. HUPPERT AND JOHN R. LISTER

Institute of Theoretical Geophysics, Department of Applied Mathematics and Theoretical Physics, University of Cambridge, CMS, Wilberforce Road, Cambridge, CB3 0WA, UK

(Received 4 June 2010; revised 3 August 2010; accepted 16 September 2010)

We consider the propagation of a buoyancy-driven gravity current in a porous medium bounded by a horizontal, impermeable boundary. The current is fed by a constant flux injected at a point and leaks through a line sink at a distance from the injection point. This is an idealized model of how a fault in a cap rock might compromise the geological sequestration of carbon dioxide. The temporal evolution of the efficiency of storage, defined as the instantaneous ratio of the rate at which fluid is stored without leaking to the rate at which it is injected, is of particular interest. We show that the 'efficiency of storage' decays like $t^{-2/5}$ for times t that are long compared with the time taken for the current to reach the fault. This algebraic decay is in contrast to the case of leakage through a circular sink (Neufeld *et al., J. Fluid Mech.*, vol. 2010) where the efficiency of storage decays more slowly like $1/\ln t$. The implications of the predicted decay in the efficiency of storage are discussed in the context of geological sequestration of carbon dioxide. Using parameter values typical of the demonstration project at Sleipner, Norway, we show that the efficiency of storage should remain greater than 90 % on a time scale of millennia, provided that there are no significant faults in the cap rock within about 12 km of the injection site.

Key words: gravity currents, porous media

1. Introduction

Recently, the study of flow in porous media has received renewed impetus because of field trials in which carbon dioxide (CO_2) is pumped into aquifers (Bickle *et al.* 2007) – the so-called geological sequestration of CO_2. It is hoped that if these trials are extended, it may be possible to sequester large quantities of CO_2, thereby mitigating the effects of climate change. Indeed, Pacala & Socolow (2004) suggested that this method alone might feasibly supply one 'wedge' out of the seven required to reduce CO_2 levels sufficiently to stabilize global temperatures.

A review of the fluid mechanics of propagation and leakage of gravity currents in porous media, with particular reference to carbon sequestration, is given in Part 1 of this paper (Neufeld *et al.* 2010). In brief, carbon sequestration consists of pumping CO_2 into a brine-saturated aquifer. At the typical temperatures and pressures within these aquifers, CO_2 becomes a supercritical fluid. The injected CO_2 remains buoyant with respect to the ambient brine and thus rises until it encounters a relatively impermeable

† Email address for correspondence: dominic.vella@cantab.net

cap rock (e.g. a shale layer), at which point it begins to spread laterally as a gravity-driven current. Given the large volumes of CO_2 that need to be sequestered, it is likely that during this spreading phase the current may encounter a fault in the overlying cap rock through which it is able to leak. In this article, we analyse the coupling between the propagation of the current and leakage through a linear fracture. The question of primary concern is whether the presence of a leakage pathway seriously compromises the efficacy of geological storage. One simple measure is the *efficiency of storage*, E_s, which was defined in Part 1 (Neufeld *et al.* 2010) as the instantaneous proportion of injected material that is stored and not leaked, i.e.

$$E_s = \frac{q - q_l}{q}, \tag{1.1}$$

where q is the injection flux and q_l is the leakage flux.

Previous studies of the effects of localized fractures on the efficiency of storage in other geometries were reviewed in Part 1. In these studies, it was found that at times, t, large compared with that taken for a gravity current to reach the sink, a steady state develops in the neighbourhood of the source and sink. In this steady state, the input flux is balanced at leading order by the leakage flux. However, far from the inner source–sink region, the current continues to evolve owing to the (decreasing) flux that escapes the sink. Matching the outer evolving current onto the inner steady state allows this flux, and hence the efficiency of storage, to be determined.

For the case of two-dimensional propagation and leakage (Pritchard 2007; Neufeld, Vella & Huppert 2009), it was found that $E_s \propto t^{-1/2}$ for $t \gg 1$. In Part 1 we considered injection from a point source near a circular sink and showed that in this case $E_s \propto (\ln t)^{-1}$ for $t \gg 1$. From these two examples it is clear that the geometry of the leakage pathway affects the quantitative behaviour of E_s at late times. In this article, we are concerned with determining the temporal evolution of E_s for the case of leakage occurring along a line sink some distance away from a point source.

The plan of the article is as follows. We present the theoretical formulation of the problem in § 2, before considering the long-time behaviour of the system using asymptotic and numerical techniques in § 3. We then consider the implications of our results for the geological sequestration of CO_2 in § 4, and conclude in § 5.

2. Theoretical development

2.1. *Geometry*

We consider the flow resulting from a point source that injects a constant flux q of liquid with density $\rho + \Delta\rho$ and dynamic viscosity μ into a semi-infinite porous medium of permeability k already saturated with a liquid of density ρ (see figure 1). The porous medium is bounded below by a horizontal plane at $z = 0$, which causes the injected liquid to spread out to form a gravity current. (The behaviour of this dense current is equivalent to a situation in which relatively buoyant fluid is injected beneath a cap rock, as is typical in the carbon sequestration projects that motivate this study.) The bounding plane acts as an impermeable barrier, confining the current to the region $z > 0$. To model the effect of a linear fault or fissure, we assume that the bounding plane is impermeable everywhere except along a line sink of width $w \ll x_s$, situated a distance x_s from the point source, which allows material to leak from the current. We orient our Cartesian coordinate system in such a way that the point source is situated at $\boldsymbol{x} = (-x_s, 0)$ and the centreline of the sink is given by $x = 0$.

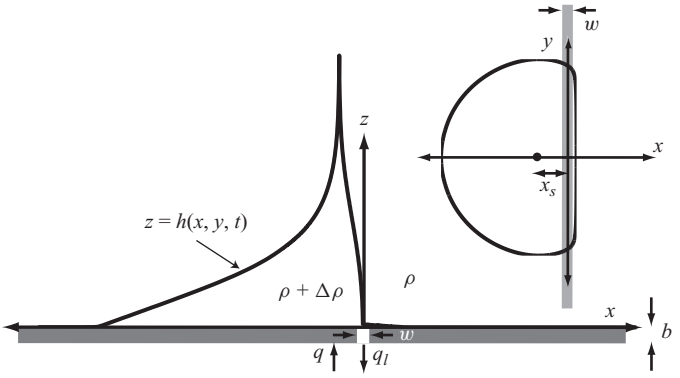

FIGURE 1. Sketch of the spreading of a dense gravity current within a porous medium in which a line sink at $x = 0$ allows fluid to leak from the current. The inset shows a planview of the spreading current along with the position of the point source and sink (grey line). The profile in the main figure shows a cross-section through a typical current taken along the x-axis. The vertical scale in this cross-section has been exaggerated for clarity.

For simplicity, we shall assume that the flow of the ambient fluid plays no role in the motion of the injected fluid because the porous medium is semi-infinite. In addition, we assume that the interface between the injected liquid and the ambient liquid is sharp and given by $z = h(x, y, t)$. For the case of CO_2 injected into brine, this latter assumption is unlikely to be satisfied because the effects of a viscosity contrast between the two fluids and surface tension are likely to lead to complicated interfacial shapes and multiphase flow. Nevertheless, we expect to gain physical insights from this simplified system that may be applied to more realistic models of CO_2 sequestration. Moreover, the effects of fingering are reduced in buoyancy-driven flow (see Lake 1989, for example).

2.2. *Leakage and propagation*

Following the approach of previous authors (Pritchard 2007; Neufeld *et al.* 2009, 2010), we assume that the leakage flow is driven by the hydrostatic overpressure, $\Delta\rho g h(x, y, t)$, through a passage of permeability k_s in a barrier of thickness b. Using the equations for flow in a porous medium (see Bear 1988; Phillips 2009, for example), the Darcy velocity within the sink is

$$v_s(x, y, t) = -\frac{k_s}{\mu}\frac{\Delta\rho g}{b}h(x, y, t) \quad (|x| < w/2). \tag{2.1}$$

Elsewhere in the current, the flow is predominantly horizontal so that the driving pressure is approximately hydrostatic. It is thus the overpressure caused by the density difference, $\Delta\rho g h$, that drives the propagation of the current. The Darcy velocity within the medium is therefore $k\Delta\rho g\nabla h/\mu$ and we may use the conservation of mass to confirm that the thickness of the current $h(x, y, t)$ evolves according to

$$\frac{\partial h}{\partial t} - \gamma\nabla\cdot(h\nabla h) = -\gamma\frac{k_s}{k}\frac{h}{b}\mathscr{F}(x; w), \tag{2.2}$$

where $\gamma = k\Delta\rho g/\phi\mu$ is the characteristic buoyancy velocity within the porous medium. The right-hand side of (2.2) represents localized leakage through the sink and

$$\mathscr{F}(x; w) = \begin{cases} 0, & |x| > w/2 \\ 1, & |x| < w/2 \end{cases} \tag{2.3}$$

is the box-car function of width w centred on the line $x = 0$.

The evolution of the current according to (2.2) is subject to the boundary conditions

$$\lim_{r\to 0}\left[2\pi r\gamma h\frac{\partial h}{\partial r}\right]=-q \quad \text{and} \quad [\boldsymbol{n}\cdot(\gamma h\nabla h)]_{\boldsymbol{r}_n}=0, \tag{2.5}$$

with $r^2=(x+x_s)^2+y^2$. These conditions impose a constant flux at the source and zero flux through the perimeter of the current (given by $\boldsymbol{x}=\boldsymbol{r}_n$), respectively.

The natural horizontal length scale is the distance x_s from the source to the sink, as shown in Part 1. We therefore use x_s to scale all horizontal distances. With this rescaling, it is natural to scale the height of the current with h^* and time with t^*, where

$$h^*=(q/\gamma)^{1/2} \quad \text{and} \quad t^*=\frac{x_s^2}{(q\gamma)^{1/2}}. \tag{2.6}$$

Using these scalings, we find that the strength of the sink is characterized by the parameter

$$\lambda=\frac{k_s}{k}\frac{x_s^2}{b(q/\gamma)^{1/2}}. \tag{2.7}$$

The propagation of the current is then governed by the dimensionless evolution equation

$$\frac{\partial h}{\partial t}-\nabla\cdot(h\nabla h)=-\lambda h\mathscr{F}(x;\epsilon), \tag{2.8}$$

where $\epsilon=w/x_s$ is the dimensionless width of the sink. The dimensionless boundary conditions are

$$\lim_{r\to 0}\left[2\pi rh\frac{\partial h}{\partial r}\right]=-1 \quad \text{and} \quad [\boldsymbol{n}\cdot(h\nabla h)]_{\boldsymbol{r}_n}=0, \tag{2.9a,b}$$

where $r^2=(x+1)^2+y^2$ in (2.9a).

When the width of the sink is small, $\epsilon\ll 1$, its effect is more naturally viewed by integrating both sides of (2.8) over $-\epsilon/2\leqslant x\leqslant\epsilon/2$. Taking the limit $\epsilon\to 0$, we find that

$$0=\int_{-\epsilon/2}^{\epsilon/2}\frac{\partial h}{\partial t}\,\mathrm{d}x=\frac{1}{2}\int_{-\epsilon/2}^{\epsilon/2}\left(\frac{\partial^2 h^2}{\partial x^2}+\frac{\partial^2 h^2}{\partial y^2}\right)\mathrm{d}x-\lambda\int_{-\epsilon/2}^{\epsilon/2}h\,\mathrm{d}x, \tag{2.10}$$

and thus obtain a flux jump condition across the sink

$$\frac{1}{2}\left.\frac{\partial h^2}{\partial x}\right|_{0^-}^{0^+}=\bar{\lambda}\bar{h}(0,y), \tag{2.11}$$

where $\bar{\lambda}=\epsilon\lambda$ and $\epsilon\bar{h}(0,y)=\int_{-\epsilon/2}^{\epsilon/2}h\,\mathrm{d}x$. Equation (2.11) shows that the flux per unit length leaking through the line sink at position y is $\bar{\lambda}\bar{h}(0,y)$. By integrating (2.11) along the length of the sink, we find that the efficiency of storage

$$E_s=1-\bar{\lambda}\int_{-\infty}^{\infty}\bar{h}(0,y)\,\mathrm{d}y. \tag{2.12}$$

2.3. *Numerical solutions*

The numerical code described in Appendix A of Part 1 (based on an alternating-direction implicit scheme) was modified to solve (2.8)–(2.9a,b) with leakage occurring from the line $x=0$ (rather than from a circular sink); the width of the sink is equal to the grid spacing, $\epsilon=\Delta x$. The numerical results presented here were obtained

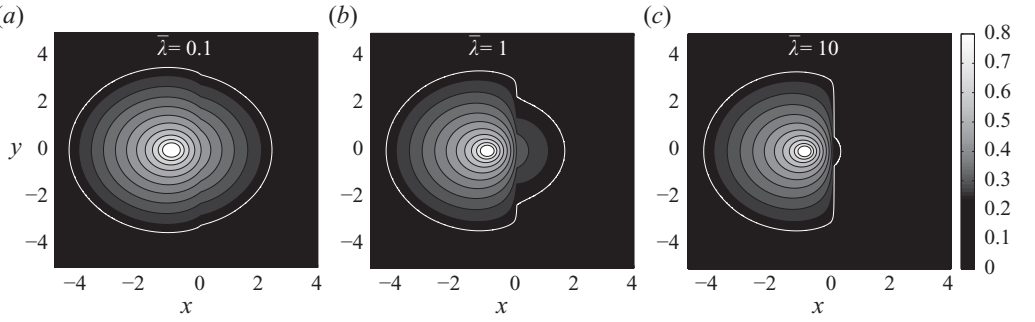

FIGURE 2. (*a–c*) Contour plots showing the shapes of currents with different values of $\bar{\lambda}$ at time $t = 10$. The value of $\bar{\lambda}$ is given in each panel. In each case, the source is positioned at $(-1, 0)$ and the sink lies along the line $x = 0$.

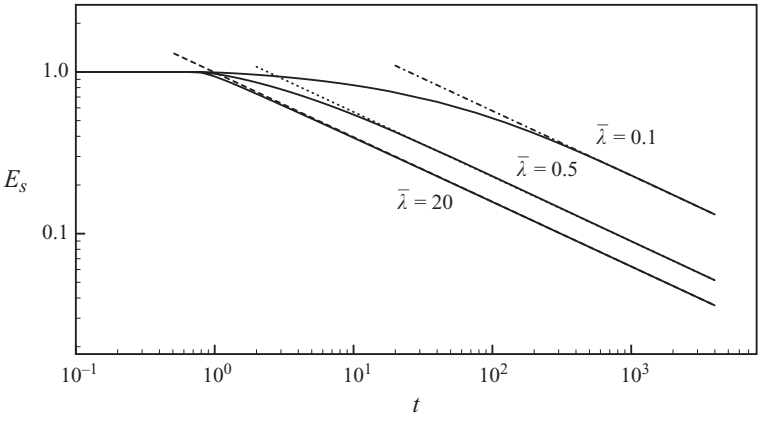

FIGURE 3. Numerical results showing the efficiency of storage, E_s, as a function of time on logarithmic scales. The non-solid lines are fits of the numerical data to the relationship $E_s = c_s t^{-2/5}$ using the last tenth of the data (i.e. largest times).

with a spatial resolution $\Delta x = 1/201$ for $-3 < x < 1$ and $-2 < y < 2$, and a stretched resolution elsewhere, as described in Appendix A of Part 1.

Our numerical results show that the current initially spreads axisymmetrically until it encounters the sink. Figure 2 shows contour plots of the current some time after it has reached the sink for three different values of $\bar{\lambda}$. These contour plots show that for small sink strengths, $\bar{\lambda} \ll 1$, the current spreads past the sink with a relatively small perturbation to its axisymmetric shape, whereas for large sink strengths, $\bar{\lambda} \gg 1$, the current only spreads a limited distance past the sink. This qualitative picture persists at later times. Furthermore, we find that the height of the current reaches a steady value close to the source–sink pair. However, the current continues to spread away from the source and the maximum radial extent of the current appears to be asymptotically proportional to $t^{2/5}$.

A quantity of considerable practical interest is the efficiency of storage, E_s, defined in (1.1). Figure 3 shows the dependence of E_s on time from simulations with three different values of $\bar{\lambda}$. We see that, for $t \gg 1$, $E_s \propto t^{-2/5}$ in each case with a prefactor that depends on the value of $\bar{\lambda}$.

3. Asymptotic efficiency of storage

In this section we use asymptotic methods to explain the algebraic decay of E_s at large times that is observed in figure 3. These asymptotic methods are based on the following physical picture (cf Pritchard 2007; Neufeld *et al.* 2009, 2010): as the evolution of the current proceeds, we expect that the height of fluid above the sink will increase. Thus the leakage flux will also increase until, in the limit of large times $t \gg 1$, it approximately balances the input flux. The solution will then consist of an approximately steady inner region $x^2+y^2=O(1)$ and an outer region $x^2+y^2 \gg 1$ (fed by the small difference between the input and leakage fluxes) in which the current continues to evolve. We therefore consider these two regions separately and then match them to obtain an asymptotic description of the evolution of E_s. We begin with the inner steady-state problem.

3.1. *Inner steady state*

Neglecting the time dependence in (2.8), we find that the profile of the inner steady-state region is given by the solution of

$$\nabla^2 h^2 = 0, \tag{3.1}$$

that accounts for a point source at $(x, y)=(-1, 0)$ as described by (2.9*a*) and leakage of an equal flux along the line sink located at $x=0$, as described by (2.11).

Since h^2 satisfies Laplace's equation in two dimensions, the steady-state problem is analogous to the three-dimensional electrostatic problem of a line charge near a plane (see Bleaney & Bleaney 1976, for example), albeit with an unusual nonlinear, mixed boundary condition at this plane. Motivated by the electrostatic analogue, we make an ansatz for the profile of the steady-state current of the form

$$2\pi h(x, y)^2 = \begin{cases} \ln\left[\dfrac{(x-1)^2+y^2}{(x+1)^2+y^2}\right] + \phi_-(x, y), & x < 0, \\ \phi_+(x, y), & x > 0. \end{cases} \tag{3.2}$$

Here the form for $x<0$ has been written as a superposition of a point source at $(-1, 0)$, an image point sink at $(1, 0)$ and a non-singular correction ϕ_-. Clearly, the functions $\phi_\pm(x, y)$ must be harmonic by (3.1). We define $\phi_0(y)=2\pi h(0, y)^2$, and note that

$$\phi_0(y) = \phi_+(0, y) = \phi_-(0, y). \tag{3.3}$$

We obtain an equation for $\phi_0(y)$ by substituting the ansatz (3.2) into the jump condition (2.11) to find that

$$\left.\frac{\partial \phi_+}{\partial x}\right|_{x=0} - \left.\frac{\partial \phi_-}{\partial x}\right|_{x=0} + \frac{4}{1+y^2} = \left(2^3\pi\right)^{1/2} \bar{\lambda} \phi_0^{1/2}. \tag{3.4}$$

By introducing the Fourier transform of $\phi_0(y)$ the boundary conditions (3.3) and (3.4) may be used to give information throughout the domain . We define the transform by

$$\tilde{\phi}_0(k) = \frac{1}{2\pi} \int_{-\infty}^{\infty} \mathrm{e}^{-\mathrm{i}ky} \phi_0(y)\, \mathrm{d}y. \tag{3.5}$$

To satisfy Laplace's equation away from $x=0$, we must have

$$\phi_\pm(x, y) = \int_{-\infty}^{\infty} \tilde{\phi}_0(k) \exp\left(\mathrm{i}ky \mp |k|x\right) \mathrm{d}k, \tag{3.6}$$

which transforms (3.4) into the integral equation

$$\left(2\pi\right)^{1/2}\bar{\lambda}\widetilde{\phi_0^{1/2}} = \exp\left(-|k|\right) - |k|\tilde{\phi}_0. \tag{3.7}$$

Solution of this equation is important in determining the dependence of the long-term efficiency of storage on the strength of the sink $\bar{\lambda}$.

Anticipating that the temporal dependence of the efficiency of storage can be found by matching the inner steady state to a spreading outer current, we now consider the outer limit of this inner solution. We first note that when $|x| \gg 1$ the exponential decay in (3.6) means that the integral will be dominated by small k. We can therefore perform a Taylor series of the integrand about $k = 0$. For large, positive x this expansion gives

$$2\pi h^2 = \phi_+ \sim \tilde{\phi}_0(0;\bar{\lambda}) \int_{-\infty}^{\infty} \exp(\mathrm{i}ky - |k|x)\,\mathrm{d}k = 2\tilde{\phi}_0(0;\bar{\lambda})\frac{x}{x^2+y^2}. \tag{3.8}$$

For large, negative x we find that

$$2\pi h^2 \sim \tilde{\phi}_0(0;\bar{\lambda}) \int_{-\infty}^{\infty} \exp(\mathrm{i}ky + |k|x)\,\mathrm{d}k - \frac{4x}{x^2+y^2} = -\frac{x}{x^2+y^2}[4 + 2\tilde{\phi}_0(0;\bar{\lambda})]. \tag{3.9}$$

Hence, the far-field of the inner steady state is characterized by

$$h \sim \begin{cases} (A_+|\cos\theta|/r)^{1/2}, & x > 0, \\ (A_-|\cos\theta|/r)^{1/2}, & x < 0, \end{cases} \tag{3.10}$$

as $r \to \infty$, where

$$A_+(\bar{\lambda}) = \frac{\tilde{\phi}_0(0;\bar{\lambda})}{\pi}, \quad A_-(\bar{\lambda}) = \frac{2 + \tilde{\phi}_0(0;\bar{\lambda})}{\pi}. \tag{3.11}$$

From the behaviour of (3.10), we see that the outer problems for $x > 0$ and $x < 0$ can only differ through the coefficients $A_{\pm}$. It is thus possible to rescale the problems, yielding a single outer problem on a half-space.

3.2. *The outer current and the asymptotic efficiency of storage*

Far from the source–sink region, flow proceeds as a gravity current fed by a dipolar source. The evolution of the current is governed by the partial-differential equation

$$\frac{\partial h}{\partial t} = \frac{1}{2}\nabla^2 h^2, \tag{3.12}$$

which can be written in scaling terms as

$$h/t \sim h^2/r^2. \tag{3.13}$$

For the solution of (3.12) to match onto the inner steady state, which is given asymptotically by (3.10), we must have that

$$h \sim (A/r)^{1/2} \tag{3.14}$$

as $r \to 0$, where

$$A = \begin{cases} A_+, & -\pi/2 \leqslant \theta \leqslant \pi/2, \\ A_-, & \pi/2 \leqslant \theta \leqslant 3\pi/2. \end{cases} \tag{3.15}$$

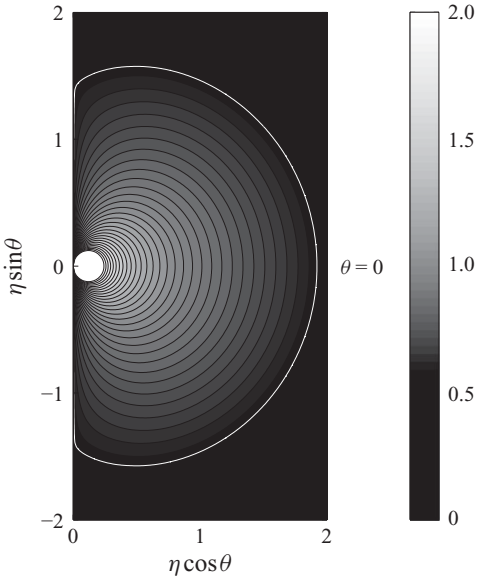

FIGURE 4. Contour plot of the outer similarity solution $H(\eta, \theta)$ to (3.17)–(3.19). The outer edge of the current $\eta_N(\theta)$ is shown by the white curve. Contours are plotted at equal intervals of 0.0666. The total volume of the similarity solution is $\tilde{V} = 2.38$. The solution for the physical outer gravity current is obtained by rescaling this solution using (3.16) with A_+ for $x > 0$ and its reflection with A_- for $x < 0$ (cf. figure 2).

These scaling relations imply that $h \sim (A^2/t)^{1/5}$ and $r \sim (At^2)^{1/5}$ and so it is natural to seek a similarity solution of the form

$$h(r, t) = \frac{A^{2/5}}{t^{1/5}} H(\eta, \theta), \tag{3.16}$$

where $\eta = r(At^2)^{-1/5}$. Substituting the similarity ansatz (3.16) into the governing equation (3.12), we find that

$$-\frac{1}{5}H - \frac{2}{5}\eta\frac{\partial H}{\partial \eta} = \frac{1}{2\eta^2}\frac{\partial^2 H^2}{\partial \theta^2} + \frac{1}{2\eta}\frac{\partial}{\partial \eta}\left(\eta\frac{\partial H^2}{\partial \eta}\right), \tag{3.17}$$

which must be solved subject to the boundary conditions that

$$H(\eta, \theta) \to \left(\frac{|\cos\theta|}{\eta}\right)^{1/2} \quad \text{as} \quad \eta \to 0, \tag{3.18}$$

and

$$H = 0 \quad (\theta = \pm\pi/2). \tag{3.19}$$

The boundary condition (3.18) arises from matching to the far-field behaviour of the inner steady state, which is given by (3.10). The boundary condition (3.19) arises from the leakage boundary condition (2.11) as follows: in scaling terms (2.11) reads $\bar{h}^2/r \sim \bar{\lambda}\bar{h}$. However, because $h^2 \ll h$ and $r \gg 1$ in the outer region, it follows that $\bar{h} \ll h$ and hence we find that $H = 0$ along the sink, and hence (3.19).

The similarity solution is shown in figure 4 for $-\pi/2 \leqslant \theta \leqslant \pi/2$. This was obtained by numerically evolving a time-dependent form of (3.17) with the boundary condition (3.19) imposed and an input flux at the origin. The input flux was rescaled to satisfy

(3.18). The numerical solution of this problem rapidly approaches a steady-state solution demonstrating also that this steady state is stable. Note that the solution for the physical outer gravity current is obtained by rescaling this solution using (3.16) with A_+ for $x > 0$ and its reflection in the y-axis with A_- for $x < 0$. The difference in the values of A_+ and A_- is responsible for the asymmetry in the shape of the currents observed in figure 2.

We may now calculate the efficiency of storage, E_s. Recalling that E_s, defined by (1.1), is the difference between the source and leakage fluxes, we write

$$E_s = \frac{q - q_l}{q} = \frac{\partial}{\partial t}\left\{\int_0^{2\pi}\int_0^{r_N} h(r,t) r \,\mathrm{d}r \,\mathrm{d}\theta\right\}. \tag{3.20}$$

Substituting the similarity solution for h from (3.16) and (3.15), we find that

$$E_s = c_s t^{-2/5}, \tag{3.21}$$

where

$$c_s(\bar{\lambda}) = \tfrac{3}{5}\tilde{V}(A_+^{4/5} + A_-^{4/5}) \tag{3.22}$$

and

$$\tilde{V} = \int_{-\pi/2}^{\pi/2}\int_0^{\eta_N} H(\eta,\theta)\eta \,\mathrm{d}\eta \,\mathrm{d}\theta \approx 2.38 \tag{3.23}$$

is the volume in the outer similarity solution of (3.17)–(3.19), see figure 4, which was determined numerically.

Thus far, we have found that the efficiency of storage decays algebraically like $t^{-2/5}$ for $t \gg 1$. This is in agreement with the numerical results presented in figure 3 for a wide range of values of $\bar{\lambda}$. Figure 3 also shows that the prefactor in this decay, c_s, varies with the sink strength $\bar{\lambda}$.

3.3. *Asymptotic leakage as a function of sink strength*

In order to determine $c_s(\bar{\lambda})$ from (3.22), we need to calculate $A_\pm(\bar{\lambda})$ from $\tilde{\phi}_0(0;\bar{\lambda})$ and (3.11). We therefore turn our attention to determining the value of $\tilde{\phi}_0(0;\bar{\lambda})$ by using a combination of steady-state numerical calculations and asymptotic analysis of the limiting cases $\bar{\lambda} \gg 1$ and $\bar{\lambda} \ll 1$. We then compare the results of this analysis with the coefficient c_s found from the long-time limit of the full time-dependent calculations.

An estimate of $\tilde{\phi}_0(0;\bar{\lambda})$ was found numerically from the solution of the inner steady-state problem described by (3.1) subject to the boundary condition (2.11). The quantity $\tilde{\phi}_0(0;\bar{\lambda})$ can be computed from the numerical solution using

$$\tilde{\phi}_0(0;\bar{\lambda}) = \int_{-\infty}^{\infty} h(0,y)^2 \,\mathrm{d}y. \tag{3.24}$$

The solid curve in figure 5 shows the result of substituting the value of $\tilde{\phi}_0(0;\bar{\lambda})$ found in this way into (3.11) and (3.22) to obtain $c_s(\bar{\lambda})$. We see that this result is in excellent agreement with fits to the long-time behaviour of E_s found in numerical solutions of the full time-dependent problem (shown by solid circles in figure 4). These two computational approaches can also be compared to asymptotic results in the limits $\bar{\lambda} \gg 1$ and $\bar{\lambda} \ll 1$.

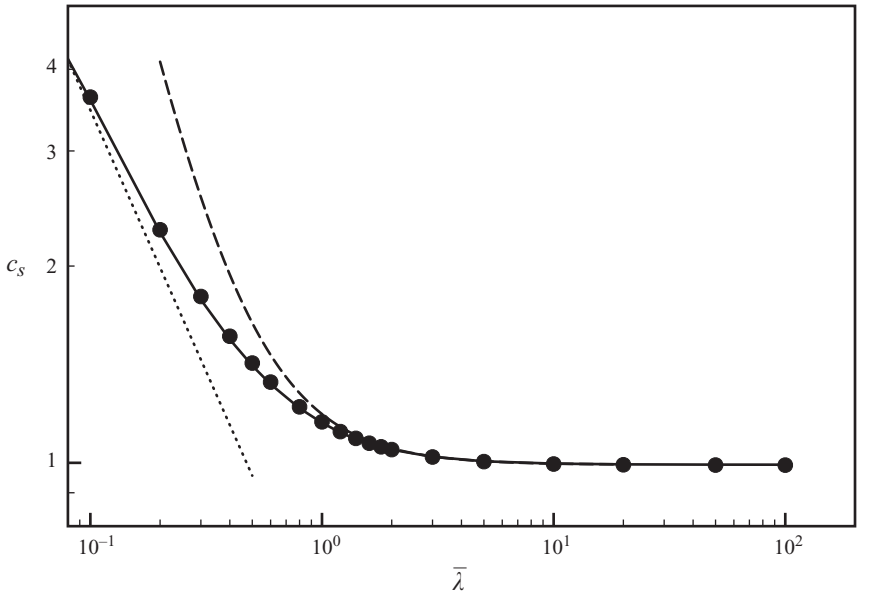

FIGURE 5. The dependence of the coefficient c_s on the sink strength $\bar{\lambda}$. Results obtained from simulations (solid circles) are in excellent agreement with the theoretical prediction (solid curve) obtained by numerical solution of the inner steady state to find $\tilde{\phi}_0(0;\bar{\lambda})$ and the outer similarity solution to find $\tilde{V}$. The asymptotic results from (3.39) for $\bar{\lambda} \ll 1$ (dotted) and from (3.30) for $\bar{\lambda} \gg 1$ (dashed) are shown. We note that, as $\bar{\lambda} \to \infty$, $c_s \to (3\tilde{V}/5)(2/\pi)^{4/5} \approx 0.99$.

3.3.1. *The limit* $\bar{\lambda} \gg 1$

For $\bar{\lambda} \gg 1$ we consider the solution of (3.7) directly. To make analytical progress, we use the convolution theorem for Fourier transforms,

$$\tilde{\phi}_0(k;\bar{\lambda}) = \int_{-\infty}^{\infty} \widetilde{\psi}(k';\bar{\lambda})\widetilde{\psi}(k-k';\bar{\lambda})\,\mathrm{d}k', \tag{3.25}$$

where $\psi(y) = \left[\phi_0(y)\right]^{1/2}$, to eliminate $\tilde{\phi}_0(k;\bar{\lambda})$ in favour of $\widetilde{\psi}(k;\bar{\lambda})$ and thus rewrite (3.7) as

$$(2\pi)^{1/2}\bar{\lambda}\widetilde{\psi} = -|k| \int_{-\infty}^{\infty} \widetilde{\psi}(k-k')\widetilde{\psi}(k')\,\mathrm{d}k' + \exp(-|k|). \tag{3.26}$$

In the asymptotic limit $\bar{\lambda} \gg 1$, we may seek a solution as a power series in $\bar{\lambda}^{-1}$. The series takes the form

$$\widetilde{\psi}(k;\bar{\lambda}) = \frac{f_{-1}(k)}{\bar{\lambda}} + \frac{f_{-3}(k)}{\bar{\lambda}^3} + O(\bar{\lambda}^{-5}), \quad \text{and} \quad \tilde{\phi}_0(k;\bar{\lambda}) = \frac{g_{-2}(k)}{\bar{\lambda}^2} + \frac{g_{-4}(k)}{\bar{\lambda}^4} + O(\bar{\lambda}^{-6}). \tag{3.27}$$

Substituting these forms into (3.26), we find that

$$f_{-1}(k) = \exp(-|k|)/(2\pi)^{1/2}, \tag{3.28}$$

and, from (3.25), that

$$g_{-2}(k) = f_{-1} * f_{-1} = \frac{1+|k|}{2\pi}\exp(-|k|). \tag{3.29}$$

These results may in turn be used to determine $f_{-3}(k)$. In principle, this iterative procedure could be repeated to give successively higher-order terms in the expansion. However, the quantity of real interest is $\tilde{\phi}_0(0;\bar{\lambda})$, which we calculate to leading order as

$$\tilde{\phi}_0(0;\bar{\lambda}) = \frac{1}{2\pi\bar{\lambda}^2} + O(\bar{\lambda}^{-4}). \tag{3.30}$$

This asymptotic result can be used, along with (3.22), to calculate c_s in the limit $\bar{\lambda} \gg 1$. The resulting solution is shown in figure 5 by the dashed curve, and is in excellent agreement with both numerical calculations for $\bar{\lambda} \gtrsim 1$. The limiting case, $\bar{\lambda} \to \infty$, when the resistance to flow within the sink tends to zero is of special interest. In this limit, the long-term efficiency of storage still decays as $t^{-2/5}$ but is now determined solely by the flow field between the source and sink with coefficient $c_s \to (3\tilde{V}/5)(2/\pi)^{4/5} \approx 0.99$.

3.3.2. *The limit* $\bar{\lambda} \ll 1$

In the limit of small sink strength, we expect the steady state to extend to large distances in order for the source flux to balance the leakage. Hence we define a rescaled coordinate $\boldsymbol{X} = \bar{\lambda}\boldsymbol{x}$. The minimum distance from the source to the sink is then given by $\bar{\lambda}$. In the limit $\bar{\lambda} \ll 1$ we must therefore solve the problem

$$\nabla^2\phi = 0, \tag{3.31}$$

$$\left[\frac{\partial\phi}{\partial X}\right]_{0-}^{0+} = (2^3\pi)^{1/2}\phi^{1/2} \quad (x = 0), \tag{3.32}$$

$$\phi \to -\ln R \quad \text{as} \quad R \to 0, \tag{3.33}$$

where $R^2 = X^2 + Y^2$ and, to leading order, the point source lies on the line sink. This solution must, however, still recover the correct far-field limit. Thus, for $R \gg 1$ we can write

$$\phi = \sum_{n=1}^{\infty} B_n R^{-n} \begin{cases} \cos n\theta & X > 0 \\ \cos n(\pi - \theta) & X < 0. \end{cases} \tag{3.34}$$

Hence

$$\left[\frac{\partial\phi}{\partial X}\right]_{0-}^{0+} = \frac{2B_1}{R^2} + O(R^{-4}) \tag{3.35}$$

and along the sink, where $\theta = \pm\pi/2$, we have

$$\phi^{1/2} = \left(-\frac{B_2}{R^2} + \frac{B_4}{R^4} + O(R^{-6})\right)^{1/2}. \tag{3.36}$$

Using (3.32), we find that $B_2 = 0$ and $B_4 = B_1^2/2\pi$. An estimate for B_1 is found numerically by considering the far-field behaviour of the numerical solution to (3.31)–(3.33). We find that $B_1 \approx 0.803$.

In the limit $\bar{\lambda} \ll 1$, $R \gg 1$ we find

$$2\pi h^2 = \phi \sim \frac{B_1\cos\theta}{R} = \frac{B_1\cos\theta}{\bar{\lambda}r}. \tag{3.37}$$

Thus, from (3.10) we see that

$$A_{\pm} = \frac{B_1}{2\pi}\bar{\lambda}^{-1} + O(1). \tag{3.38}$$

The function $c_s(\bar{\lambda})$ for $\bar{\lambda} \ll 1$ may then be determined by substituting (3.38) into (3.22). We find that

$$c_s = \frac{3}{5}\tilde{V}\left(\frac{B_1}{2\pi}\right)^{4/5}\bar{\lambda}^{-4/5} + O(\bar{\lambda}^{1/5}) \approx 0.55\bar{\lambda}^{-4/5}, \tag{3.39}$$

which is shown by the dotted line in figure 5.

4. Geophysical relevance

Our analysis of the spread and leakage of a gravity current in a porous medium with a line sink has shown that, under the assumptions of our model, the efficiency of storage decays towards zero algebraically with time. This could be a cause for concern when attempting to store positively buoyant fluids (such as CO_2) within an aquifer since a steady state may be reached in which material leaks from the fissure at the same rate as it is injected at the source. However, on the time scale of centuries to millennia, secondary trapping mechanisms exist (e.g. the dissolution of CO_2 in ambient brine and capillary trapping in the pore spaces), which act to store the liquid in the porous medium permanently and negate the risk of leakage. The relevant question then becomes: does the primary trapping provided by the almost impermeable cap rock last sufficiently long for other, secondary, trapping mechanisms to take over and store CO_2 permanently?

A natural measure of the time scale over which the cap rock traps material is the time taken for the efficiency of storage to decay to 90 %, which we denote by t_{90}. Figure 6(*a*) shows t_{90} as a function of the sink strength $\bar{\lambda}$. It is interesting to note that as $\bar{\lambda} \to \infty$, t_{90} tends to a constant value $t_{90} \approx 1.1$. This gives us a worst-case scenario: even with unrestricted leakage our model predicts that the storage efficiency is above 90 % for dimensionless times $t < 1.1$. In dimensional terms, the storage efficiency will remain above 90 % provided that

$$t < 1.1\frac{x_s^2}{(q\gamma)^{1/2}} = 1.1x_s^2\left(\frac{\phi\mu}{kq\Delta\rho g}\right)^{1/2}. \tag{4.1}$$

As an example of how the worst-case scenario given by (4.1) might be used in practice, we consider the demonstration project in the Sleipner field beneath the North Sea. Here, Statoil injects supercritical CO_2 with dynamic viscosity $\mu = 4.5 \times 10^{-5}$ Pa s and density $\rho \approx 505\,\mathrm{kg\,m^{-3}}$ into an aquifer with permeability $k \approx 10^{-12}\,\mathrm{m^2}$ and porosity $\phi = 0.3$ at an approximately constant flux $q = 1\,\mathrm{MT\,yr^{-1}} \approx 0.062\,\mathrm{m^3\,s^{-1}}$ (Bickle *et al.* 2007). Using these values along with (4.1), we find that $x_s > 12.5\,\mathrm{km}$ is sufficient to guarantee that $t_{90} > 10^3$ years for *any* size of fault. A more nuanced view can be found by calculating for a given fracture size, w/b, and distance from the source, x_s, whether t_{90} is greater or smaller than 10^3 years. Since these are the two significant unknowns for a given injection project, a plot of $(x_s, w/b)$ parameter space may prove useful in assessing leakage risks. Such a plot is shown in figure 6(*b*) for values representative of the Sleipner project. In physical terms, this shows which fault widths w (measured relative to the cap rock depth, b) can be tolerated at a distance x_s from the injection point without compromising storage on the time scale of 10^3 years.

5. Conclusions

The buoyancy-driven propagation of an injected liquid within a saturated porous medium bounded by an impermeable barrier has been considered for the case in which

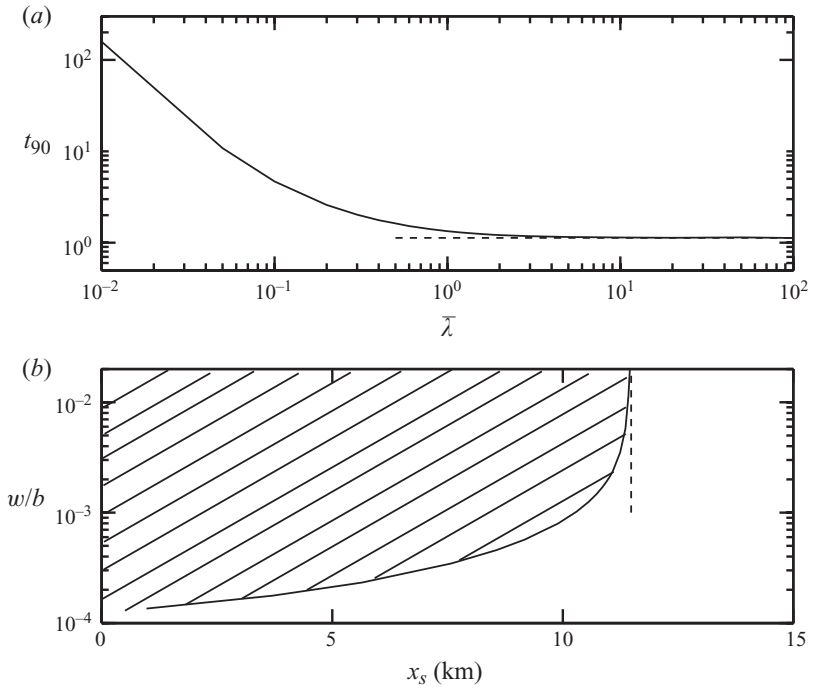

FIGURE 6. (*a*) Numerical results showing the time taken for the efficiency of storage E_s to decay to 90 %, t_{90}, as a function of the sink strength $\bar{\lambda}$ (solid curve) together with the lower bound $t_{90} \approx 1.1$ valid for $\bar{\lambda} \gg 1$ (dashed line). (*b*) The regions of $(x_s, w/b)$ parameter space for which $t_{90} > 10^3$ years (unhatched region) and $t_{90} < 10^3$ years (hatched region) separated by $t_{90} = 10^3$ years (solid curve), obtained numerically. The dashed vertical line shows the asymptote of $t_{90} = 10^3$ years, which corresponds to $\bar{\lambda} \to \infty$.

the impermeable layer contains a localized fault along a line at a minimum distance x_s from the point of injection. The dimensionless governing equations for buoyancy-driven flow through the reservoir and leakage through the sink were presented in § 2, and we then considered the long-time behaviour of this model using asymptotic and numerical methods in § 3. The behaviour of such currents can be characterized by an efficiency of storage, E_s, which our analysis showed decays algebraically in time like $t^{-2/5}$, with a prefactor that depends on the strength of the sink (parametrized by $\bar{\lambda}$). Another important characteristic of storage was introduced: the time taken t_{90} for E_s to decay to 90 %. Crucially, t_{90} is bounded below by a constant for all sink strengths $\bar{\lambda}$, allowing a worst-case scenario to be considered. The geophysical significance of these results was considered in § 4. It was shown that there must be no fault within a critical distance of the injection point if significant quantities of liquid are to remain trapped by the cap rock long enough for secondary trapping mechanisms to store them permanently. Other effects, such as the finite size and heterogeneity of the porous medium, capillary effects and viscosity contrasts also need to be considered.

D. V. is supported by the 1851 Royal Commission and an Oppenheimer Early Career Research Fellowship. J.A.N. is grateful for support through a Lloyd's Tercentenary Fellowship and a Leverhulme Early Career Fellowship. Partial support of the research of H.E.H. comes from a Wolfson Royal Society merit award.

REFERENCES

Bear, J. 1988 *Dynamics of Fluids in Porous Media*. Dover.

Bickle, M., Chadwick, A., Huppert, H. E., Hallworth, M. A. & Lyle, S. 2007 Modelling carbon-dioxide accumulation at Sleipner: implications for underground carbon storage. *Earth Planet. Sci. Lett*. **255**, 164–176.

Bleaney, B. I. & Bleaney, B. 1976 *Electricity and Magnetism*. Oxford University Press.

Lake, L. 1989 *Enhanced Oil Recovery*. Prentice Hall.

Neufeld, J. A., Vella, D. & Huppert, H. E. 2009 The effect of a fissure on storage in a porous medium. *J. Fluid Mech.* **639**, 239–259.

Neufeld, J. A., Vella, D., Huppert, H. E. & Lister, J. R. 2010 Leakage from a gravity current in a porous medium. Part 1. A localized sink. *J. Fluid Mech.* doi:10.1017/S002211201000488X.

Pacala, S. & Socolow, R. 2004 Stabilization wedges: solving the climate problem for the next 50 years with current technologies. *Science* **305**, 968–972.

Phillips, O. M. 2009 *Geological Fluid Dynamics: Sub-Surface Flow and Reactions*. Cambridge University Press.

Pritchard, D. 2007 Gravity currents over fractured substrates in a porous medium. *J. Fluid Mech.* **584**, 415–431.